Polymer 51 (2010) 482–491

Contents lists available at ScienceDirect

Polymer

journal homepage: www.elsevier.com/locate/polymer

The design of well-defined PDMS–Magnetite complexes

W.C. Miles [a,c], J.D. Goff [b,c], P.P. Huffstetler [b,c], O.T. Mefford [b,c], J.S. Riffle [b,c], R.M. Davis [a,c,*]

[a] Department of Chemical Engineering, Virginia Tech, Blacksburg, VA 24061, USA
[b] Department of Chemistry, Virginia Tech, Blacksburg, VA 24061, USA
[c] The Macromolecules and Interfaces Institute, Virginia Tech, Blacksburg, VA 24061, USA

ARTICLE INFO

Article history:
Received 25 June 2009
Received in revised form
7 November 2009
Accepted 13 November 2009
Available online 2 December 2009

Keywords:
Magnetite
Polydimethylsiloxane brush
Particle size distribution

ABSTRACT

Magnetic nanoparticles have numerous applications, particularly in biological systems for drug delivery, cell targeting, and as MRI contrast agents. This paper addresses the synthesis and characterization of well-defined magnetite nanoparticles coated with tricarboxylate-functional polydimethylsiloxane (PDMS) oligomers of varying molecular weight. Two methods – co-precipitation of iron chlorides and high-temperature reduction of iron(III) acetylacetonate – were used to synthesize the magnetite nanoparticles and compared. Through implementation of a polymer brush model, it was determined that the co-precipitation synthesis method required multiple magnetic separations and significant material loss to produce a well-defined particle distribution. Conversely, the high-temperature synthesis method showed a well-defined particle distribution without any magnetic separation. Through adjustment of critical design parameters such as polymer loading and molecular weight, the diameters of the complexes were predicted to within seven percent of experimental values. This demonstrates a tool for the design of sterically-stabilized single–particle complexes with a specifically tailored particle size.

1. Introduction

Magnetite nanoparticles have many uses in biomaterials due to their resistance to oxidation and their low cytotoxicities [1,2]. Some of these biological applications include uses in cellular therapy, cellular targeting, tissue repair, drug delivery, magnetic resonance imaging (MRI), and hyperthermia [3–14]. Biocompatible macromolecules can be adsorbed on the magnetite surface, which allows specific functionality to be built into the polymer–magnetite complexes, such as targeting and imaging agents [1,2,15–19].

Synthesis of magnetic particles can be achieved through various methods, including wet grinding, co-precipitation, microemulsion and inverse microemulsion methods, thermolysis of organometallic compounds, and reduction of metal salts in aqueous solution [20]. The particles must then either be coated with a surfactant to provide steric stability or have their surface modified to produce a repulsive electrostatic force to prevent aggregation [20–22]. One approach has been to attach soluble non-ionic polymers to a magnetite surface to form a polymer brush. The steric repulsion provided by both the enthalpic and entropic energies arising from confinement of the chains upon the approach of two particles significantly increases colloidal stability [23]. Various polymer stabilizers have been used in conjunction with magnetite, including poly(vinyl pyrrolidone), dextran, polydimethylsiloxane, poly(ethylene oxide), and poly (propylene oxide-*b*-ethylene oxide) diblock copolymers [2,14,24–29]. Through adjustment of polymer loading and molecular weight, extension of the brush can be controlled to produce a stable dispersion [30].

Much of the research currently focused on nanoparticle dispersions for biological applications uses an approach that focuses on efficacy of commercial materials or particle systems that show some degree of aggregation in solution [31–37]. Emerging biomedical applications will require precise control of the size and breadth of the nanoparticle distribution both for determination of biodistribution after administration as well as dose control. Additionally, to our knowledge, no general methodology exists to design polymer–nanoparticle complexes with control of particle sizes within a few nanometers.

Therefore, the focus of our work has been to develop a methodology to allow for the precise design of polymer–nanoparticle complexes. Magnetite nanoparticles stabilized by various molecular weight PDMS stabilizers were used in this study. Two methods were used to synthesize the polymer–magnetite complexes and the materials were compared. The first method, co-precipitation of iron chloride salts with base, required extensive magnetic separation due to aggregation. Through application of a polymer brush model

* Corresponding author. Virginia Tech, Department of Chemical Engineering, 133 Randolph Hall, Blacksburg, VA 24061, USA. Tel.: +540 231 4578; fax: +540 231 5022.
E-mail address: rmdavis@vt.edu (R.M. Davis).

0032-3861/$ – see front matter © 2009 Elsevier Ltd. All rights reserved.
doi:10.1016/j.polymer.2009.11.022

adapted from Vagberg et al. [38] and comparison to dynamic light scattering (DLS) measurements, we have been able to determine when separation is necessary and how much material must be removed to achieve a well-defined narrow size distribution.

Due to significant material loss during the magnetic separation steps, a different synthetic route, thermal reduction of organometallic compounds, was also utilized to prepare complexes. The brush model was also applied to this system and comparison to DLS measurements confirmed that no magnetic separation was necessary for this system. This brush model has previously been successfully applied to polyether–magnetite complexes [30]. Thus, it appears that the application of this polymer brush model is applicable to significantly different polymer–nanoparticle systems. Additionally, we now have a methodology to determine whether a system is comprised of sterically-stabilized single particles in suspension and to predict the size of the complex. This will allow for design of various polymer–nanoparticle complexes for biomedical applications.

2. Experimental

2.1. Materials

Hexamethylcyclotrisiloxane (D_3, Gelest, Inc., 98%) was dried over calcium hydride prior to use. Cyclohexane (Fischer Scientific, HPLC grade) was stirred with concentrated sulfuric acid for 48 h, washed with deionized water until neutral and dried over magnesium sulfate. The cyclohexane was then stirred over calcium hydride, fractionally distilled under vacuum, stored over sodium in a nitrogen atmosphere, and distilled just prior to use. Tetrahydrofuran (THF, EMD Chemicals, 99.5%) was refluxed over sodium with benzophenone until the solution reached a deep purple, and fractionally distilled just prior to use. Toluene (Burdick and Jackson, 99.9%) was used as received. 2,2′-Azobisisobutyronitrile (AIBN, 98%), n-butyllithium (2.5 M solution in hexanes) and mercaptoacetic acid (97%) were purchased from Aldrich and used as received. Trivinylchlorosilane (Gelest Inc., 95%) and trimethylchlorosilane (Gelest Inc., 99%) were used as received. Ammonium hydroxide (VWR International) was diluted with Millipore water to yield a 50/50 v/v solution and deoxygenated with nitrogen just prior to use. Iron (III) chloride hexahydrate (≥98%) and iron (II) chloride tetrahydrate (99%) were obtained from Sigma–Aldrich and were ground into fine powders and stored under nitrogen prior to use. Iron (III) acetylacetonate ($Fe(acac)_3$) was purchased from Aldrich and used as received. Hydrochloric acid (EMD, 12.1 M) was added to deionized (DI) water to yield a 3.0 M solution. DI water was deoxygenated just prior to use. Dichloromethane was obtained from EMD Chemicals and used as received. Iron granules (Alfa Aesar, 1–2 mm, 99.98%) were washed repeatedly with a variety of solvents to remove any coating on the surface and subsequently dried overnight in a vacuum oven at 40 °C. The iron granules (6 g) were then placed into a 3 mL syringe packed with glass wool to obtain magnetic separation columns. NdFeB doughnut-shaped magnets were purchased from Engineered Concepts and had an outer diameter of 2.54 cm, an inner diameter of 1.26 cm and were 0.65 cm thick. Magnetic separation columns were prepared by magnetizing the iron-granule-packed syringe with the doughnut-shaped magnets.

2.2. Synthesis and functionalization of trivinylsilyl-terminated PDMS

The synthesis of trivinyl-terminated PDMS was carried out as described previously [39,40]. Various molecular weights were prepared in an analogous manner with appropriate ratios of initiator to monomer to control chain length. The living anionic polymerizations were monitored using ^{1}H NMR and ^{1}H NMR confirmed the expected chemical structure.

The PDMS oligomers were then functionalized with three carboxylic acid groups on one terminus via a thiol-ene addition of mercaptoacetic acid across the vinylsilane endgroups as described previously [39,40]. ^{1}H NMR was used to observe the quantitative disappearance of the vinyl proton peaks (~6 ppm), indicating completion of the thiol-ene functionalization reaction. The reaction mixture was concentrated under vacuum at 60 °C, and the product was dissolved in methanol (10 mL). DI water was added dropwise to the solution until a white solid precipitate formed, which was collected via vacuum filtration. This precipitation was repeated 3×, and the recovered polymer was dried under vacuum overnight at 80 °C.

2.3. Magnetite synthesis via co-precipitation of iron chlorides with ammonium hydroxide

Synthesis of magnetite nanoparticles and subsequent adsorption of a representative carboxylate-functional PDMS dispersion stabilizer onto the nanoparticle surfaces was achieved via the following procedure. The experimental conditions describe a method to obtain a PDMS stabilizer–magnetite complex comprised of ~30 wt% magnetite and ~70 wt% PDMS as the dispersion stabilizer. Magnetite nanoparticles were prepared using a chemical co-precipitation of iron salts. Iron (III) chloride hexahydrate (3.50 g, 0.013 mol) and iron (II) chloride tetrahydrate (1.28 g, 0.0064 mol) were weighed into separate round-bottom flasks, and each was dissolved in 20 mL of deoxygenated water. The two iron salt solutions were then added to a 500 mL, three-necked, round-bottom flask fitted with an Ultra-Turrax T25 Digital Homogenizer, a pH electrode and a nitrogen purge. The iron salts solution was stirred at 13,000 rpm with the homogenizer and the ammonium hydroxide solution (~20 mL) was added via syringe until the rapidly stirring solution turned black and reached a pH of 9–10. The PDMS dispersion stabilizer (3.5 g) was dissolved in dichloromethane (60 mL), and this solution was added to the basic magnetite dispersion and stirred for 30 min. Aqueous HCl (3.0 M) was then slowly added until a slightly acidic pH was obtained (~12 mL was required to reach pH 5–6). The heterogeneous dispersion was stirred for 1 h, then transferred to a separatory funnel and allowed to separate for 24 h. The dichloromethane layer containing the PDMS–magnetite complex was collected. The dichloromethane layer containing the PDMS–magnetite complex was dried with magnesium sulfate, vacuum-filtered, and concentrated under vacuum. The recovered PDMS–magnetite nanoparticle fluid was washed 3× with methanol (15 mL each) and dried under vacuum overnight at 80 °C. TGA was used to determine the composition of the PDMS–magnetite nanoparticle fluid.

2.4. Magnetite synthesis via reduction of Fe (III) acetylacetonate

Magnetite nanoparticles were synthesized using a reduction method adapted from Pinna et al. [41] Fe (III) acetylacetonate (2.14 g, 8.4 mmol) and benzyl alcohol (45 mL, 0.43 mol) were added to a 250 mL, three-necked round-bottom flask equipped with a water condenser and overhead mechanical stirrer. N_2 was passed through the solution for 1 h. While stirring under N_2, the solution was heated to 100 °C for 4 h, then the temperature was increased to 205 °C at a rate of ~25 °C h^{-1}. Following 24 h at 205 °C, the reaction was cooled to room temperature, then the magnetite particles were collected with a magnet and the benzyl alcohol was decanted. The magnetite nanoparticles were washed 3× with acetone, then were dispersed in chloroform (20 mL) containing oleic acid (0.3 g).

Table 1
Trivinylsilyl-terminated PDMS molecular weights and distributions.

Targeted Trivinjl-PDMS MW	M_n (g mol^{-1})		PDI
	^{1}H NMR	GPC	
3000	3050	3150	1.08
5000	5100	4830	1.09
7000	6900	6910	1.05
10,000	10,200	9850	1.07

The solvent was removed under vacuum at room temperature, and the oleic acid-stabilized magnetite nanoparticles were washed 3× with acetone. The particles were dried under vacuum for 24 h at 25 °C. The composition of the particles obtained from thermogravimetric analysis (TGA) showed 5% organic residue to 95% magnetite.

A representative method for preparing a targeted composition of 70:30 wt:wt of a PDMS:magnetite complex is provided. Oleic acid-stabilized magnetite nanoparticles (25 mg) prepared as described above were dispersed in chloroform (10 mL) and added to a 50 mL round-bottom flask. A carboxyl-functional PDMS (58 mg) was dissolved in chloroform (10 mL) and added to the dispersion. The reaction mixture was sonicated in a VWR 75T sonicator for 16 h under N_2. The chloroform was removed via evaporation, and the resulting ferrofluid was washed 3X with methanol (15 mL each) to remove excess polymer. A magnet was utilized to collect the magnetite nanoparticles and free PDMS was decanted with the supernatant. The complexes were dried under N_2 at 25 °C and TGA was used to determine the composition of the PDMS–magnetite nanoparticle fluid.

2.5. Magnetic separations of PDMS–magnetite nanoparticle fluids

Mefford et al. described the use of magnetic separation techniques to remove aggregates from a 3000 g mol^{-1} PDMS–magnetite complex for magnetite made via the co-precipitation method [39]. In this study, removal of the slightly-aggregated complexes from the total sample was accomplished through repeated magnetic separations in the same fashion. The separation columns were comprised of iron granules tightly packed into 3 mL syringes. The syringes were 6.60 cm in length with an inner diameter of 1.00 cm. The length of the iron granules in the separation columns was approximately 2.45 cm with a diameter of 1.00 cm. Two doughnut-shaped magnets were placed around the circumferences of the iron granule-packed syringes to form the magnetic separation columns, and a Hall probe was used to measure the magnetic field generated by the separation column (~0.1 T). Great care was taken at each step of the column formation to ensure reproducibility.

Two concentrations of the PDMS–magnetite nanoparticle fluids in chloroform (1 mg mL^{-1} and 10 mg mL^{-1}) were investigated in the magnetic separation studies. The concentrated and dilute dispersions of the PDMS–magnetite complexes were passed through five magnetic separation columns. Aliquots of the PDMS–magnetite complexes were collected after the first and fifth magnetic separations and dried under vacuum at 80 °C overnight. After each magnetic separation of a PDMS–magnetite complex, the columns were washed with chloroform (~20 mL) in the absence of a magnetic field to recover the material removed from the bulk sample. The initial material, first separation, fifth separation and column-extracted materials were characterized by DLS, TEM, and TGA.

3. Characterization

Spectral analyses of compounds were performed using a Varian Unity 400 NMR and a Varian Inova 400 NMR. An Alliance Waters 2690 Separations Module with a Viscotek T60A dual viscosity detector and laser refractometer equipped with a Waters HR 0.5 + HR 2 + HR 3 + HR 4 styragel column set was used for gel permeation chromatography (GPC) analyses. GPC data were collected in chloroform at 30 °C. Data were analyzed utilizing a Universal calibration to obtain absolute molecular weights.

TGA was carried out on the tricarboxylate-functional PDMS and PDMS-stabilized magnetite nanoparticles using a TA Instruments TGA Q500. Samples were first held at 110 °C for 10 min to remove any residual solvent. Samples were then equilibrated at 30 °C and the temperature was ramped at 10 °C min^{-1} to 700 °C in a nitrogen atmosphere. Char yields were recorded at the maximum temperature. TGA was used to determine the composition of the PDMS–magnetite nanoparticle fluids.

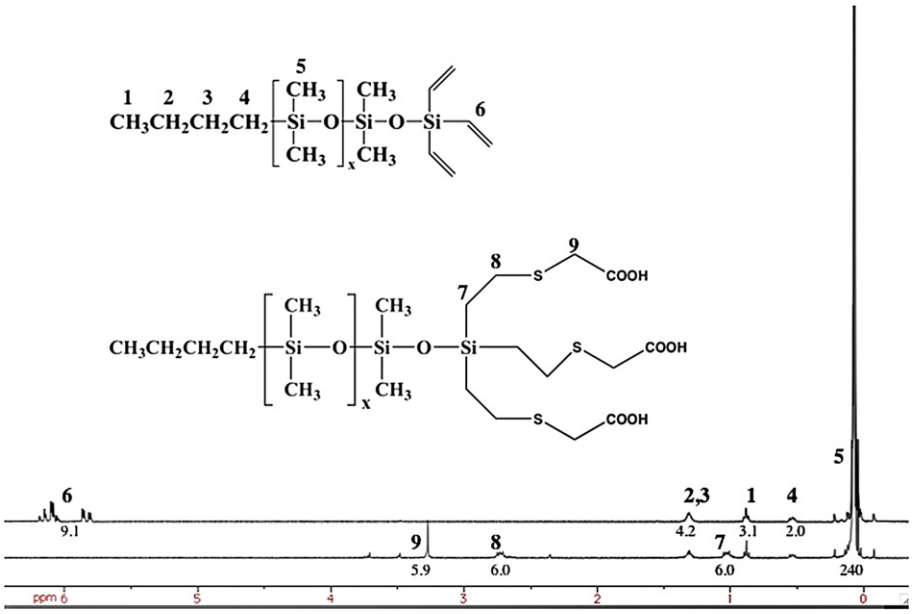

Fig. 1. ^{1}H NMR confirms the addition of mercaptoacetic acid across vinylsilane groups on a 3100 g mol^{-1} trivinylsilyl-terminated PDMS. The upper spectrum is trivinylsilyl-terminated PDMS; lower spectrum is the tricarbonylate-functional PDMS.

TEM was conducted using a Philips EM-420 field-emission-gun transmission electron microscope. Samples of the polymer–magnetite complexes were dispersed in chloroform through probe sonication and analyzed after being cast onto amorphous carbon-coated copper grids. The eucentric height and focus were set consistently for each sample. The microscope was equipped with a 2000 × 3000 pixel digital imaging system, and images were acquired at a magnification of 96 kx at a voltage of 100 kV, corresponding to a resolution of 3.7 pixels nm^{-1}. At least 2000 particles taken from five separate images were used for image analysis. Particle distribution analyses were performed using Reindeer Graphics' Fovea Pro 4 plug-in for Adobe Photoshop 7.0.

A Malvern Zetasizer NanoZS particle analyzer (Malvern Instruments Ltd, Malvern, UK) was used to conduct dynamic light scattering (DLS) experiments of the complexes in chloroform at 25 °C. A 4.0 mW, solid-state He–Ne laser at a wavelength of 633 nm was the incident light source. The NanoZS measures at a scattering angle of 173°, which reduces the effects of multiple scattering and contaminants such as dust. Malvern's Zetasizer Nano 4.2 software was used to calculate intensity, volume and number average diameters utilizing an algorithm that transforms time-varying intensities to particle diameters [42].

Powder X-Ray Diffraction (XRD) patterns were obtained using a Scintag XDS-2000 diffractometer with a Ni-filtered Cu-Kα ($\lambda = 0.154$ nm) radiation source. The patterns were obtained at a scan rate of 1.0 $2\theta\ s^{-1}$ and were scanned from 10 to 90°. Particle diameters were obtained using the Scherrer formula, which allows for estimation of particle diameter as a function of the width of the diffraction curves [43].

3.1. Density distribution model to predict sizes of the PDMS–magnetite nanoparticle complexes

Modeling of the PDMS–magnetite complexes to predict their sizes in various solutions was based on methods developed by Mefford, Zhang, and Miles [29,30,39,40]. TEM was used to image the particles and image analysis was performed on the magnetite cores (only the magnetite component of the complexes is visible by TEM). The size distribution of the magnetite was fitted with a Weibull probability distribution ($P(a)$) as shown in Equation (1).

$$P(a) = \frac{c}{b}\left(\frac{a}{b}\right)^{c-1}\exp\left[-\left(\frac{a}{b}\right)^{c}\right] \tag{1}$$

Here, a is the particle radius and b and c are the Weibull shape and scale parameters, respectively.

The average surface area of the magnetite was calculated from the particle size distribution derived from TEM. Combining the average surface area with the average polymer loading per mass of complex (from TGA) gives an average number of chains per magnetite surface area, α, as shown in Equation (2).

$$\alpha = \frac{(1 - W_{mag})N_{Av}\rho_{mag}}{3M_n W_{mag}} \frac{\int_0^\infty a^3 P(a)dr}{\int_0^\infty a^2 P(a)dr} \tag{2}$$

Here, ρ_{mag} is the density of magnetite (5.21 $g\,cm^{-3}$), [44] W_{mag} is the weight fraction of the complex that is magnetite, N_{Av} is Avogadro's number, and M_n is the PDMS number average molecular weight. Equation (2) is slightly different than the one previously reported for reasons of self-consistency, but the difference in the number average diameter resulting from this change is less than three percent [30,39,40]. Through application of a modified version of the Vagberg density distribution model [30,38–40], the average radius of the PDMS–magnetite complexes was calculated as

$$R_m(a) = \left(\frac{8N_k f(a)^{\frac{1-\nu}{2\nu}} L_k^{1/\nu}}{4^{1/\nu}3\nu} + a^{1/\nu}\right)^{\nu} \tag{3}$$

where N_k is the number of Kuhn segments, L_k is the Kuhn length (0.81 nm) [44], υ is the Flory exponent (0.6 for a good solvent), and $f(a)$ is the number of chains per particle, which were calculated from Equation (4).

$$f(a) = 4\pi a^2 \alpha \tag{4}$$

All of the measurements were performed in chloroform, which is a good solvent for PDMS

Different modes of the complex distribution were calculated through a Weibull probability distribution fit (Equations (5), (6), and (7)) where D_n, D_v, and D_i are the number, volume, and intensity average diameters, respectively.

$$D_n = 2\int_0^\infty R_m(a)P(a)da \tag{5}$$

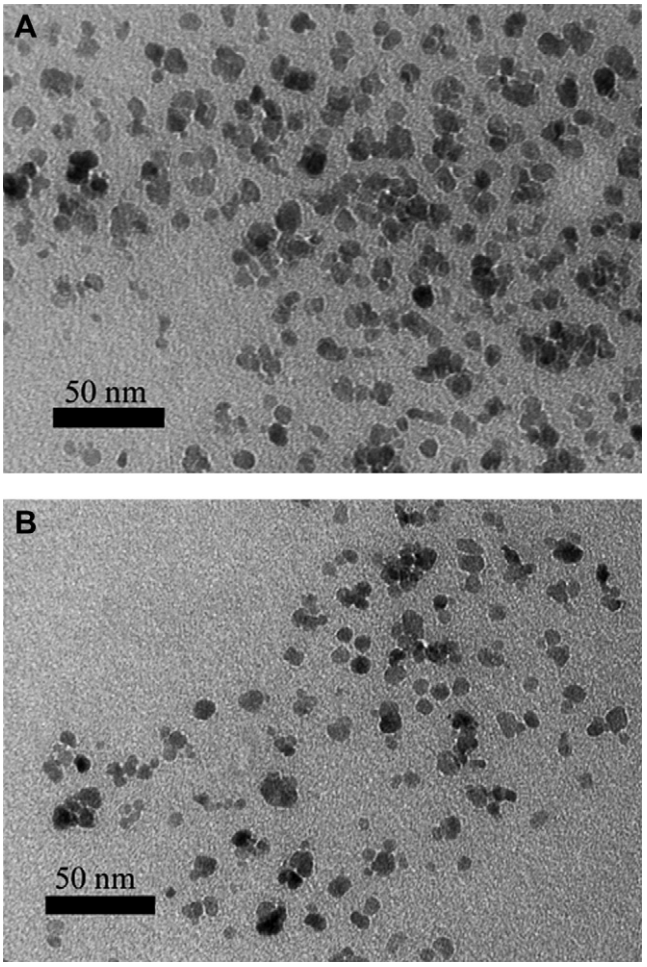

Fig. 2. TEM images of a 5100 $g\,mol^{-1}$ PDMS–magnetite complex before magnetic separation (A) and following five magnetic separations (B).

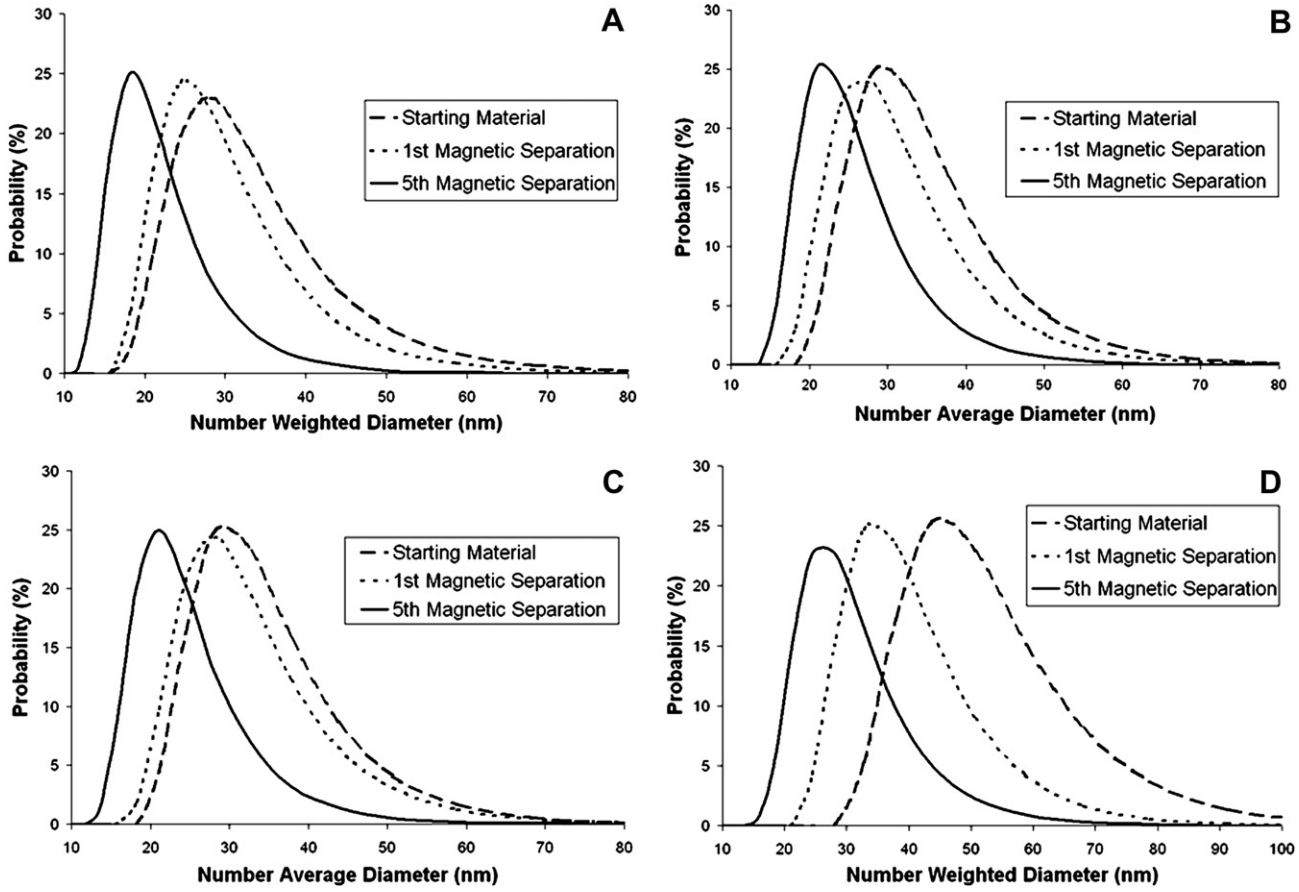

Fig. 3. The number weighted diameter distributions of the 3050 (A), 5100 (B), 6900 (C), and 10,200 g mol^{-1} (D) PDMS–magnetite complexes in chloroform at 25 °C display the effect of magnetic separation for a magnetic field above the saturation magnetization at 10 mg mL^{-1}.

$$D_v = 2\frac{\int_0^\infty R_m(a)^4 P(a)da}{\int_0^\infty R_m(a)^3 P(a)da} \quad (6)$$

$$D_i = 2\frac{\int_0^\infty R_m(a)^6 P(a)da}{\int_0^\infty R_m(a)^5 P(a)da} \quad (7)$$

For our purposes, the focus will be on the number weighted average, both from a modeling and a light scattering perspective. The reason is that of these distributions, the number weighted average is the least susceptible to aggregation. Large amounts of aggregation must be present before the number average will change significantly. Thus, comparison of a calculated number average to an experimental average from light scattering allows determination of considerable aggregation.

The brush model can also be used to calculate the pair–pair potential for polymer–particle complexes of the same size as previously described by our group [30,40]. The calculation of these potentials is described in equation (8).

$$V_{Total} = V_{vdW} + V_M + V_{ES} + V_S \quad (8)$$

V_{vdW} is the attractive potential due to van der Waal's interactions, V_M is the attractive potential produced by an applied magnetic field, V_{ES} is the repulsive potential due to electrostatic interactions, and V_S is the repulsive potential due to steric repulsion of the polymer brushes. The electrostatic potential can be calculated as

$$V_{ES} = 2\pi a\varepsilon\varepsilon_o\psi_o^2 \ln\left(1 + e^{-\kappa(r-2a)}\right) \quad (9)$$

where ε is the dielectric constant of the solvent, ε_o is the permittivity of free space, ψ_o is the surface potential, κ is the inverse Debye length, r is the center-to-center separation, and a is the particle radius [45]. However, chloroform has a significantly lower dielectric constant compared to water (4 vs. 80 at room temperature, respectively) and thus the repulsive electrostatic interaction is negligible due to the extremely small Debye length. The magnetic potential can be calculated as

$$V_M = \frac{8\pi\mu_o a^3 M^2}{9\left(\frac{h}{a}+2\right)^3} \quad (10)$$

where a is the particle radius, M is the magnetization (345,000 A m^{-1}), μ_o is the magnetic permeability in vacuum (1.26e-6 Tm A^{-1}), and h is the surface-to-surface separation of two particles [46]. The van der Waal's potential can be calculated as

$$V_{vdW} = -\frac{1}{6}A_{eff}\left(\frac{2a^2}{r^2-4a^2} + \frac{2a^2}{r^2} + \ln\left(\frac{r^2-4a^2}{r^2}\right)\right) \quad (11)$$

Table 2
Comparison of the model predictions of number average hydrodynamic diameter (±standard deviation) with experimental measurements indicate that five magnetic separations are necessary to obtain a well-defined particle size distribution.

PDMS–magnetite complex	% Magnetite	Starting material	1st separation	5th separation	Model
		DLS Dn (nm)	DLS Dn (nm)	DLS Dn (nm)	Dn (nm)
3050 g mol^{-1}	35	29.6 ± 1.7	27.0 ± 0.3	19.7 ± 0.4	18.2
5100 g mol^{-1}	29	31.0 ± 0.5	29.7 ± 1.4	20.1 ± 0.6	22.7
6900 g mol^{-1}	24	30.1 ± 2.0	30.0 ± 0.6	21.8 ± 0.8	26.5
10,200 g mol^{-1}	26	48.4 ± 1.5	36.5 ± 1.0	27.6 ± 2.6	30.0

where r is the center-to-center separation distance of two particles and a is the particle radius. A_{eff} is the effective retarded Hamaker constant calculated according to previous work [30,40].

For the case of a densely adsorbed brush layer, the steric contribution to the interaction potential may be described by the Likos expression [47].

$$V_S = \frac{5}{18}kTf(a)^{3/2}\begin{cases} -\ln\left(\frac{r}{\sigma}+\frac{1}{1+\frac{\sqrt{f(a)}}{2}}\right) & r \le \sigma \\ \frac{1}{1+\frac{\sqrt{f(a)}}{2}}\left(\frac{\sigma}{r}\right)\exp\left(-\frac{\sqrt{f(a)}}{2\sigma}(r-\sigma)\right) & r > \sigma \end{cases} \quad (12)$$

Here, r is the center-to-center separation, f(a) is the number of chains per particle, and $\sigma/2$ is the distance from the center of the core to the center of the outermost blob layer [45,47]. For this expression, σ is defined as $1.3R_g$, the radius of gyration of the ensemble [45]. Thus, determination of the onset of a sharp increase in the steric potential is determined by the R_g, which is calculated as done previously [30,40]. By taking these potential energy terms in aggregate (van der Waals, magnetic, electrostatic, and steric), a pair–pair potential energy diagram can be constructed to determine the effect of a magnetic field on the separation of these materials as a function of molecular weight.

4. Results and discussion

4.1. Synthesis of PDMS–magnetite complexes

The synthetic procedure for obtaining a tricarboxylate-functional PDMS oligomer has been previously reported [24,39]. Great care was taken to purify all solvents and reagents for the D_3 polymerizations to prevent premature termination of the growing PDMS chains. The living anionic polymerization of D_3 yielded polymers with good control over molecular weights and narrow molecular weight distributions, as confirmed by NMR and GPC (Table 1). A series of trivinylsilyl-terminated PDMS oligomers were synthesized with targeted molecular weights ranging from 3000 to 10,000 g mol^{-1}. The molecular weights obtained from GPC and NMR were in close agreement with the targeted values.

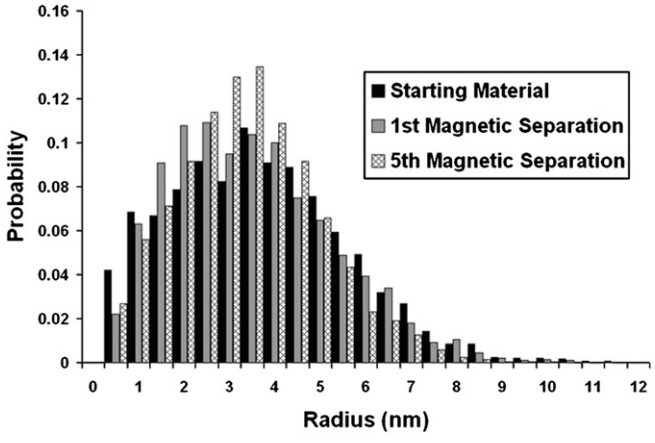

Fig. 4. Image analysis shows no significant difference between the particle size histograms for the starting material (3.4 ± 2.0 nm), first magnetic separation (3.2 ± 1.8 nm), and fifth magnetic separation (3.1 ± 1.6 nm) of the 6900 g mol^{-1} PDMS–magnetite complex.

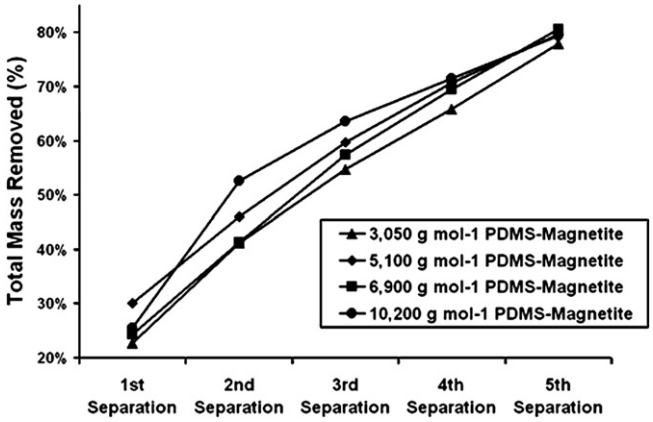

Fig. 5. For each molecular weight, approximately 80 percent of the material is removed after five separations.

Tricarboxylate-functional PDMS–magnetite dispersion stabilizers were synthesized via the ene-thiol addition of mercaptoacetic acid to the trivinylsilyl-terminated PDMS series. Complete conversion of the vinyl groups was promoted by thoroughly deoxygenating the reaction mixtures before the additions. Excess mercaptoacetic acid was removed from the polymer during isolation by precipitating the polymer into a methanol/water mixture, yielding well-defined tricarboxylate-functional PDMS oligomers. The addition of mercaptoacetic acid across the vinylsilane groups was confirmed by ^{1}H NMR (Fig. 1).

Using these polymers, PDMS–magnetite complexes were formed with compositions close to those targeted (approximately 30 wt% magnetite and 70 wt% PDMS coating) as determined by TGA.

4.2. Characterization of PDMS–magnetite complexes synthesized through co-precipitation

Due to aggregation in the system, magnetic separation was employed to remove aggregates and obtain a more defined and narrow particle size distribution. Fig. 2 shows representative images of the 5100 g mol^{-1} PDMS–magnetite complex without separation and following five magnetic separations. There are clearly fewer aggregates in the magnetically separated image than in the starting material. However, determining the degree of aggregation in either case is difficult just from images alone. DLS was then used to characterize the extent of aggregation of these materials in chloroform (a good solvent for PDMS).

Fig. 3 shows the number weighted diameter distribution from DLS of the four PDMS–magnetite complexes with differing molecular weight stabilizers during various stages of magnetic separation at a concentration of 10 mg mL^{-1}. Each of these distributions is an average of three consecutive measurements. Passing the PDMS–magnetite complexes through the separation columns removes the larger particles. Each distribution decreases both in width and

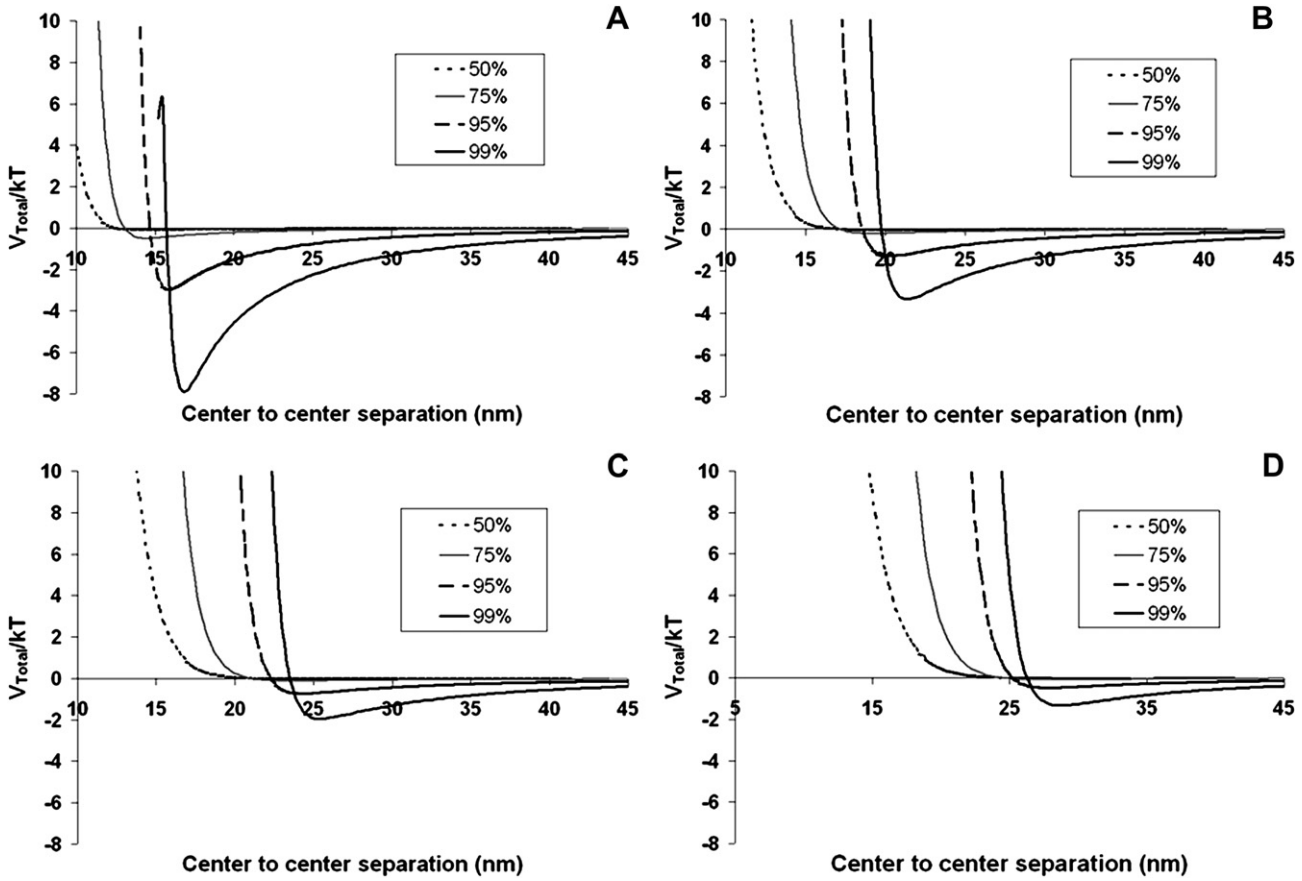

Fig. 6. Potential energy diagrams of the 3050 (A), 5100 (B), 6900 (C), and 10,200 g mol^{-1} (D) PDMS-magnetite complexes (compositions shown in Table 2) show deeper secondary minimum energy wells for the smaller polymer brush with an applied magnetic field above their saturation magnetization.

overall diameter with increasing separations, indicating that multiple separations are necessary to obtain a well-defined distribution of polymer-stabilized single magnetite nanoparticles.

This is also observed in Table 2, which shows the number average diameters predicted by the model compared to those obtained via DLS for the starting material and the material after both one and five magnetic separations for all four PDMS molecular weights. Note that these solutions were separated at a concentration of 1 mg mL^{-1}, both to assure dilute solution conditions and to prevent saturation of the magnetic separation column.

Note that the model comes into better agreement with the DLS data with an increased number of magnetic separations. This again indicates that multiple magnetic separations are necessary in order to obtain a well-defined system. This treatment does assume a constant number of chains per surface area for each magnetite particle in the distribution, irrespective of the particle size. The increased agreement between the model and the sizes measured by DLS with subsequent magnetic separations indicates that this assumption is reasonable as long as the core particle size is not affected significantly by the magnetic separation (i.e. if only aggregates are removed and not single particles).

This was confirmed through image analysis, where the size distributions of the magnetite core for the starting material, first magnetic separation, and fifth magnetic separation for the 6900 g mol^{-1} PDMS–magnetite complexes were compared as shown in Fig. 4.

This method of image analysis divides any obvious aggregates into its components, thus eliminating the complexities of determining which particles are aggregated and which are not. This allows determination of the nominal magnetite core size which does not appreciably change in the magnetic separation process. The only parameter that changes is the degree of aggregation of the system, which is reflected in the DLS measurements.

The primary issue with this separation technique is that approximately 80 percent of the material (by mass) is lost during the series of five separations at a concentration of 1 mg mL^{-1} (Fig. 5). Fig. 3 and Table 2 illustrate the need for five magnetic separations to obtain a well-defined particle system, and so a significant loss of material is inevitable regardless of molecular weight when using this method. Also, the core particle size does not change, which means that 80 percent of the material is in the form of aggregates, indicating that the synthetic procedure for making the complexes is not ideal.

Application of extended DLVO theory also confirms that the single core particles should not be appreciably separated through the magnetic fractionation step irrespective of polymer molecular weight or magnetic field strength. Examination of the pair–pair potentials for the different polymer brushes at a magnetic field strength above the saturation magnetization of the nanoparticles predicts that the majority of the material removed should be magnetite aggregates. Fig. 6 shows these potential energy diagrams generated for all four molecular weights examined in this study using extended DLVO theory with the added magnetic pair–pair potential as described previously. The potential energy diagrams were calculated for the 50th (4.1 nm), 75th (4.9 nm), 95th (6.1 nm), and 99th (6.9 nm) percentile of the core particle size distribution as determined by image analysis. A more negative secondary potential energy well indicates a propensity for aggregation of two

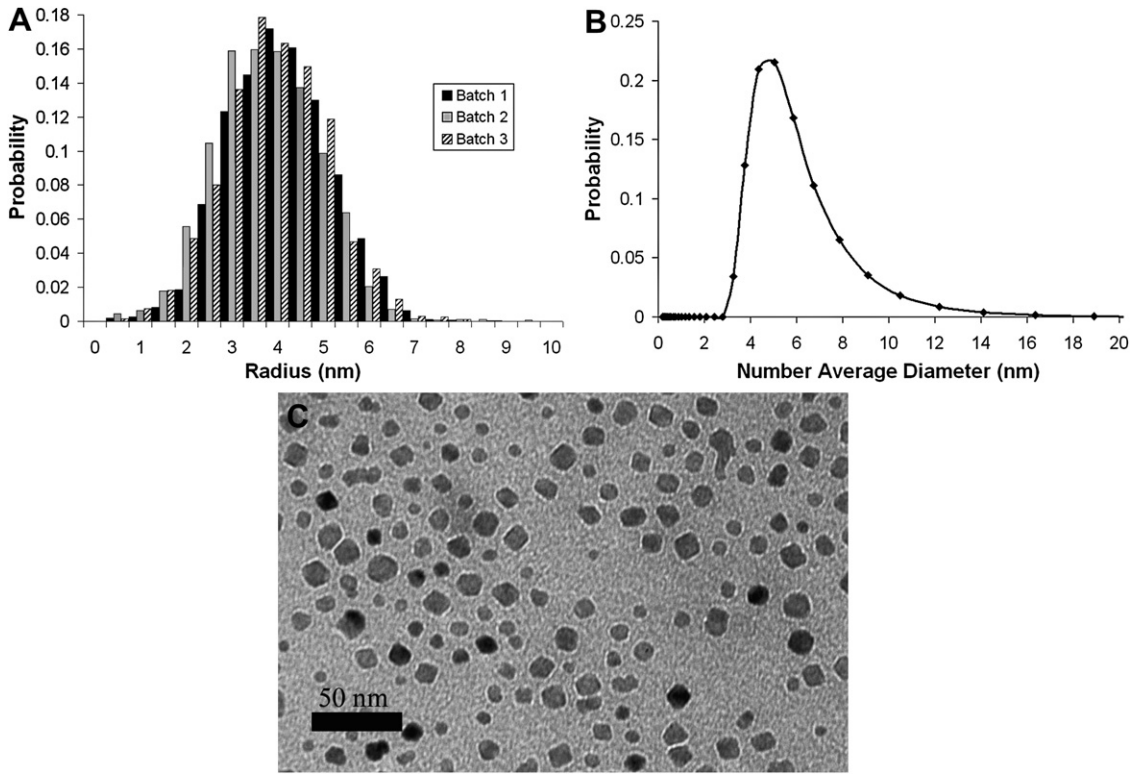

Fig. 7. TEM image analysis (A) and dynamic light scattering (B) show a narrow particle size distribution while a representative TEM image (C) shows a well-defined magnetite core.

complexes interacting with each other. As illustrated in Fig. 6, only the 99th percentile of the particle size distribution is susceptible to magnetically induced flocculation. Of the four complexes examined, only the 3050 g mol^{-1} PDMS–magnetite complex might exhibit appreciable flocculation. However, Fig. 5 indicates no appreciable difference in the % mass lost during magnetic separation. The secondary potential energy wells for all molecular weights are very similar for the 95th percentile and are identical for the 50th and 75th percentiles of the particle size distribution regardless of molecular weight. Thus, the separation profiles of each molecular weight should be mostly uniform, and the number of single particles removed from the system should be negligible, as observed by image analysis.

4.3. Characterization of PDMS–magnetite complexes synthesized through thermal reduction of Fe (acac)$_3$

Because of the issues outlined in the previous section, a more uniform magnetite size distribution was desired. This was achieved through the elevated temperature reduction of iron (III) acetylacetonate adapted from Pinna et al. [41]. Fig. 7 shows a representative TEM image of the 3050 g mol^{-1} PDM–magnetite complex as well as particle histograms for three different magnetite syntheses obtained through image analysis and a number average radius distribution from DLS, illustrating the remarkable reproducibility of the particle size distributions (radii of 3.9 ± 1.1 nm, 3.5 ± 1.2 nm, and 3.9 ± 1.2 nm for batches 1, 2, and 3, respectively). The slight increase in size observed from DLS (5.6 ± 0.9 nm) is due to the oleic acid stabilizer adsorbed to the bare magnetite during the synthesis. Additionally, XRD was performed on another magnetite batch prior to coating with oleic acid, and through application of the Scherrer equation ($D_{xRD} = 0.9\lambda/\beta\cos(\theta)$, where λ is the wavelength of radiation, β is the peak width at half-height in radians, and θ is the angle of reflection) [43], a radius of 4.1 ± 0.6 nm was obtained from five different XRD peaks. This compares favorably to the averages obtained via image analysis and DLS. Because these methods require the assumption that the particle is spherical, the consistency of the data from both image analysis and XRD supports the validity of this assumption.

Polymer–magnetite complexes were prepared with all four PDMS molecular weights. Different polymer loadings for the 3050, 5100, and 6900 g mol^{-1} PDMS–magnetite complexes were used to ensure that the model was correctly predicting the PDMS brush extension. Just as before, all DLS measurements were made in chloroform, a good solvent for PDMS. Table 3 shows a comparison of the number average diameters obtained from DLS with those predicted by the model for the PDMS–magnetite complexes for seven independent combinations of polymer molecular weight and loading.

As illustrated in Table 3, there is remarkable agreement between the DLS measurements and the model predictions for this system, especially since no adjustable parameters are used in the model. The largest deviation between the predicted and experimental values is 3.2 nm, and the average deviation is seven percent, which is on par with the error typically associated with DLS

Table 3
Comparison of the number average hydrodynamic diameters (±standard deviation) with those predicted by the model indicate a well-defined particle size distribution.

PDMS–magnetite complex	% Magnetite	DLS Dn (nm)	Model Dn (nm)
3050 g mol^{-1}	35	19.5 ± 1.9	18.1
	44	18.9 ± 0.4	17.1
5100 g mol^{-1}	21	23.7 ± 0.5	24.5
	42	21.6 ± 0.9	20.6
6900 g mol^{-1}	38	23.7 ± 0.5	23.5
	47	20.4 ± 2.1	22.0
10,200 g mol^{-1}	41	23.2 ± 1.0	26.4

measurements and previous comparisons to the model made with polyether-stabilized complexes [30]. As expected, an increase in PDMS molecular weight or a decrease in magnetite loading resulted in an increase of the complex diameter.

The accuracy of the model compared to the DLS measurements is a strong indication that the high-temperature magnetite synthetic route provides a well-defined particle size distribution. The reproducibility of different batches means that this synthetic method can be used repeatedly to obtain the same magnetite distribution, allowing for design and control of various polymer–particle properties. Most importantly, the high-temperature synthetic route requires no magnetic fractionation, which eliminates material loss associated with the co-precipitation.

5. Conclusions

Sterically-stabilized complexes comprised of PDMS and magnetite nanoparticles were synthesized using two different magnetite synthetic methods and four different PDMS molecular weights. Through comparison of a polymer brush model with DLS measurements, it was determined that the co-precipitation synthetic method resulted in aggregates. Multiple magnetic separations were necessary to obtain a well-defined narrow particle distribution and while this did produce the desired distribution, nearly 80 percent of the total starting material was lost in the separation process. Image analysis and the application of extended DLVO theory with an added magnetic pair–pair potential indicated that aggregates were the main component being removed through the magnetic separation process, and varying the molecular weight of the PDMS brush did not appreciably affect the separation profiles.

A thermolysis method that involved reduction of iron (III) acetylacetonate was implemented to produce a particle size distribution consisting of primarily single particles to eliminate the magnetic separation step. The reproducibility of this method was confirmed through analysis of TEM images for multiple magnetite batches and through X-ray diffraction. The polymer brush model was applied to these complexes and predicted the PDMS–magnetite complex sizes within seven percent of those measured by DLS for both varying molecular weight and polymer loading. This indicates that the model accurately describes how the PDMS brush extends out from the magnetite nanoparticle surface. Previous work in our group has examined the use of this model to predict the sizes of polyether–magnetite complexes with similar agreement [30]. The model includes no adjustable parameters, and predicts the sizes of significantly different types of polymer–magnetite complexes based on published values of the Flory exponent for solvent quality, the statistical polymer segment length, and the statistical number of segments per polymer chain.

Most importantly, through application and validation of this brush model, we now have a readily available methodology for the design of sterically-stabilized single–particle complexes with sizes tailored to within at least ten percent of a desired value. Additionally, the model provides a tool for determining the state of aggregation of a system in solution and whether further separation techniques are necessary to remove unwanted components. This knowledge will allow for the design of polymer–nanoparticle systems for biomedical applications with specific functionalities and the ability to determine the critical design parameters for variables such as cellular uptake and efficacy of delivery.

Acknowledgements

This material is based upon work supported in part by the Macromolecular Interfaces with Life Science IGERT of the NSF No. DGE-0333378, by DMR-0312046, and by DMR-0602932 (the NSF Materials World Network for the Study of Macromolecular Ferrofluids). We are also grateful to Bayer Materials Science for partial support of a student. Parts of this work were carried out in the Nanoscale Characterization and Fabrication Laboratory, a Virginia Tech facility operated by the Institute for Critical Technology and Applied Science. The authors thank Dr. Robert Woodward, Dr. Ted Oyama, Dr. Travis Gott, and Matthew Carroll.

References

[1] Hamoudeh M, Al Faraj A, Canet-Soulas E, Bessueille F, Leonard D, Fessi H. International Journal of Pharmaceutics 2007;338(1–2):248–57.
[2] Harris LA, Goff JD, Carmichael AY, Riffle JS, Harburn JJ, St Pierre TG, et al. Chemistry of Materials 2003;15(6):1367–77.
[3] Handgretinger R, Lang P, Schumm M, Taylor G, Neu S, Koscielnak E, et al. Bone Marrow Transplantation 1998;21(10):987–93.
[4] Olsvik O, Popovic T, Skjerve E, Cudjoe KS, Hornes E, Ugelstad J, et al. Clinical Microbiology Reviews 1994;7(1):43–54.
[5] Schoepf U, Marecos EM, Melder RJ, Jain RK, Weissleder R. Biotechniques 1998;24(4):642.
[6] Yeh TC, Zhang WG, Ildstad ST, Ho C. Magnetic Resonance in Medicine 1993;30(5):617–25.
[7] Bulte JWM, Douglas T, Witwer B, Zhang SC, Strable E, Lewis BK, et al. Nature Biotechnology 2001;19(12):1141–7.
[8] Chan DCF, Kirpotin DB, Bunn PA. Synthesis and evaluation of colloidal magnetic iron-oxides for the Site-specific radiofrequency-induced hyperthermia of cancer. 6th International Conf on magnetic fluids (Icmf 6). Paris, France; 1992. p. 374–78.
[9] Enochs WS, Harsh G, Hochberg F, Weissleder R. Jmri-Journal of Magnetic Resonance Imaging 1999;9(2):228–32.
[10] Jordan A, Scholz R, Wust P, Schirra H, Schiestel T, Schmidt H, and et-al. Endocytosis of dextran and silan-coated magnetite nanoparticles and the effect of intracellular hyperthermia on human mammary carcinoma cells in vitro. 2nd International Conference on scientific and clinical applications of magnetic carriers (SCAMC2). Cleveland, Ohio; 1998. p. 185–96.
[11] Widder KJ, Senyei AE, Ranney DF. Cancer Research 1980;40(10):3512–7.
[12] Zhang Y, Kohler N, Zhang MQ. Biomaterials 2002;23(7):1553–61.
[13] Zhao M, Beauregard DA, Loizou L, Davletov B, Brindle KM. Nature Medicine 2001;7(11):1241–4.
[14] Huffstetler PP, Miles WC, Goff JD, Reinholz CM, Carroll MRJ, Woodward RC, et al. Polymer Preprint 2008;49(2):1103–4.
[15] Cohn D, Lando G, Sosnik A, Garty S, Levi A. Biomaterials 2006;27(9):1718–27.
[16] He GS, Ma LL, Pan J, Venkatraman S. International Journal of Pharmaceutics 2007;334(1–2):48–55.
[17] Yang J, Lee H, Hyung W, Park SB, Haam S. Journal of Microencapsulation 2006;23(2):203–12.
[18] Yellen BB, Forbes ZG, Halverson DS, Fridman G, Barbee KA, Chorny M, et al. Journal of Magnetism and Magnetic Materials 2005;293(1):647–54.
[19] Yuan JJ, Armes SP, Takabayashi Y, Prassides K, Leite CAP, Galembeck F, et al. Langmuir 2006;22(26):10989–93.
[20] Odenbach S. Ferrofluids: magnetically controllable fluids and their applications. Berlin: Springer; 2002.
[21] Berkovsky B. Thermomechanics of magnetic ferrofluids: theory and applications. New York: Hemisphere Publishing Corporation; 1978.
[22] Fertman VE. Magnetic fluids guidebook: properties and applications. New York: Hemisphere Publishing Corporation; 1990.
[23] Hiemenz P, Rajagopalan R. Principles of colloid and surface chemistry. 3rd ed. New York: Marcel Dekker, Inc.; 1997.
[24] Wilson KS, Goff JD, Riffle JS, Harris LA, St Pierre TG. Polymers for Advanced Technologies 2005;16(2–3):200–11.
[25] Gossuin Y, Roch A, Muller RN, Gillis P, Lo Bue F. Magnetic Resonance in Medicine 2002;48(6):959–64.
[26] Lee H, Lee E, Kim DK, Jang NK, Jeong YY, Jon S. Journal of the American Chemical Society 2006;128(22):7383–9.
[27] Martina MS, Fortin JP, Menager C, Clement O, Barratt G, Grabielle-Madelmont C, et al. Journal of the American Chemical Society 2005;127(30):10676–85.
[28] Vadala ML, Thompson MS, Ashworth MA, Lin Y, Vadala TP, Ragheb R, et al. Biomacromolecules 2008;9(3):1035–43.
[29] Zhang QA, Thompson MS, Carmichael-Baranauskas AY, Caba BL, Zalich MA, Lin YN, et al. Langmuir 2007;23(13):6927–36.
[30] Miles WC, Goff JD, Huffstetler PP, Reinholz CM, Pothayee N, Caba BL, et al. Langmuir 2009;25(2):803–13.
[31] Batrakova EV, Kabanov AV. Journal of Controlled Release 2008;130(2):98–106.
[32] Batrakova EV, Li S, Alakhov VY, Miller DW, Kabanov AV. Journal of Pharmacology and Experimental Therapeutics 2003;304(2):845–54.
[33] Sharma AK, Zhang L, Li S, Kelly DL, Alakhov VY, Batrakova EV, et al. Journal of Controlled Release 2008;131(3):220–7.
[34] Yang Z, Sahay G, Sriadibhatla S, Kabanov AV. Bioconjugate Chemistry 2008;19(10):1987–94.

[35] Ito A, Kuga Y, Honda H, Kikkawa H, Horiuchi A, Watanabe Y, et al. Cancer Letters 2004;212(2):167–75.
[36] Babic M, Horak D, Trchova M, Jendelova P, Glogarova K, Lesny P, et al. Bioconjugate Chemistry 2008;19(3):740–50.
[37] Horak D, Babic M, Jendelova P, Herynek V, Trchova M, Pientka Z, et al. Bioconjugate Chemistry 2007;18(3):635–44.
[38] Vagberg LJM, Cogan KA, Gast AP. Macromolecules 1991;24(7):1670–7.
[39] Mefford OT, Carroll MRJ, Vadala ML, Goff JD, Mejia-Ariza R, Saunders M, et al. Chemistry of Materials 2008;20(6):2184–91.
[40] Mefford OT, Vadala ML, Goff JD, Carroll MRJ, Mejia-Ariza R, Caba BL, et al. Langmuir 2008;24(9):5060–9.
[41] Pinna N, Grancharov S, Beato P, Bonville P, Antonietti M, Niederberger M. Chemistry of Materials 2005;17(11):3044–9.
[42] Zetasizer nano series user manual. Worcestershire: Malvern Instruments, Ltd.; 2005.
[43] Cullity BD. Elements of X-ray diffraction. 2nd ed. Menlo Park: Addison-Wesley; 1978.
[44] CRC handbook of chemistry and physics. Boca Raton, FL: CRC Press; 2006–2007.
[45] Jusufi A, Watzlawek M, Lowen H. Macromolecules 1999;32(13):4470–3.
[46] Plaza RC, de Vicente J, Gomez-Lopera S, Delgado AV. Journal of Colloid and Interface Science 2001;242(2):306–13.
[47] Likos CN. Soft Matter 2006;2(6):478–98.